NEAR-WALL STREAK MODIFICATIONS BY SPANWISE OSCILLATORY WALL MOTIONS

Emile Touber
Department of Aeronautics, Imperial College London, London SW7 2AZ, U.K.
e.touber@imperial.ac.uk

Michael A. Leschziner
Department of Aeronautics, Imperial College London, London SW7 2AZ, U.K.
mike.leschziner@imperial.ac.uk

ABSTRACT

Direct numerical simulations for channel flow have been performed and analysed in an effort to illuminate the fundamental mechanisms contributing to the reduction in turbulent friction drag, observed when an oscillatory spanwise wall motion is imposed. A range of statistical data are discussed, and structural features are investigated by reference to the response of streak properties to the oscillatory forcing. The unsteady cross-flow straining is shown to significantly distort the near-wall turbulence structures, leading to a pronounced reduction in the wall-normal momentum exchange in the viscous sublayer, hence disrupting the turbulence contribution to the wall shear stress. Furthermore, a modulating "top-to-bottom" effect, associated with large-scale outer-layer structures, is highlighted and deemed responsible for the observed reduction in the actuation efficiency as the Reynolds number is increased.

INTRODUCTION

Efforts to develop strategies for reducing friction drag constitute a particularly active research area in aerodynamics. A major motivation for this work is societal pressure to reduce fuel consumption in the transport sector. One interesting approach to achieve significant net reductions in turbulent skin friction is through oscillatory wall motions (see Quadrio et al., 2009, and references therein). While gross reduction levels of up to 40% are often reported (Jung et al., 1992), maximum net power savings, when accounting for the power needed to move the wall, are closer to 18% in the case of spanwise oscillations combined with streamwise wave motions (see Quadrio et al., 2009). Although these figures pertain to low-Reynolds-number channel flows, the technique nevertheless attracts major interest in the transport sector.

Lateral wall oscillations are known to lead to the formation of a so-called Stokes boundary layer. In the case of a laminar channel flow, the Stokes layer is limited to the spanwise velocity component (denoted $\tilde{w}$ herein), which is fully decoupled from both the streamwise (u) and wall-normal (v) velocity components. In the case of turbulent channel flows, however, the modulation of the turbulent stochastic fluctuations (u'', v'', w'') can contribute to the diffusion of the phase fluctuations ($\tilde{u}$, $\tilde{w} - \tilde{v}$ is strictly zero) making $\tilde{u}$ and $\tilde{w}$ depart from their respective laminar values. In cases where maximum drag reduction is achieved, the phase modulation of the turbulence is weak, and the laminar solution for the phase fluctuations is an excellent approximation (see Touber and Leschziner, 2011). Weak periodic modulation of the turbulence does not imply the absence of modification of the turbulence, however, as manifested by the modification of the mean-velocity profile through significant modifications of the shear stress. This suggests that the Stokes layer affects directly the stochastic part of the velocity fluctuations, and it is important, therefore, to investigate the interaction of the Stokes-layer with the turbulence structure.

The present study aims to shed light on the dynamic mechanisms through which spanwise wall oscillations can lead to efficient modifications (specifically damping) of the near-wall turbulence structure. In particular, attention focuses on the detailed mechanisms by which oscillation affects the strength and organisation of the streaky structures (defined here as regions of velocity deficits with respect to the local mean value), held to be central to drag reduction.

METHODOLOGY AND CONFIGURATIONS

This study employs direct numerical simulations (DNS) of turbulent-channel flows, performed using a variant of the in-house incompressible Navier–Stokes solver "Stream-LES" (Temmerman et al., 2003). This is based on a general non-orthogonal-grid, block-structured, finite-volume method with a fully co-located storage. The algorithm advances the velocity field in time by means of a fractional-step method incorporating fourth-order approximations for the fluxes and a third-order Gear-like scheme shown to possess advantageous stability and accuracy properties relative to a corresponding second-order time-advancement scheme (Fishpool and Leschziner, 2009). Zero divergence is secured by solving the pressure-Poisson equation, which combines the application of an implicit successive over-relaxation method with a

multigrid scheme. Pressure-velocity decoupling, arising from the fully-collocated storage of velocity and pressure, is counteracted by employing the so-called Rhie & Chow interpolation scheme.

Results reported herein arise from simulations at $Re_\tau \equiv u_\tau h/\nu = 500$ where u_τ is the friction velocity and h the channel half height. The grid is $4\pi h \times 2h \times 2\pi h$ in size with $384 \times 256 \times 384$ grid points. The forcing is a simple sine wave applied to both walls (in phase) with amplitude $W_\mathrm{m}^+ \equiv W_\mathrm{m}/u_\tau = 12$ and period $T^+ \equiv Tu_\tau^2/\nu$ set to 100 and 200. In all cases, the flow in the channel is maintained by enforcing a constant mass flow rate.

RESULTS AND DISCUSSION

Preliminary observation of flow structures

One key characteristic feature of near-wall turbulence structures is the presence of elongated regions of alternative streamwise-velocity excess and defect, referred to as near-wall streaks, as shown in figure 1a (where the visualisation window width is about 3000 wall units). These streaks, which weaken substantially with forcing, are statistically separated by a distance λ_z^+ of order 10^2 wall units (based on the two-point-correlation function of u' in the spanwise direction). Figure 1a also brings to light the existence of outer "super-streaks" separated by a distance about five times larger than that pertaining to the near-wall streaks (i.e. $\lambda_z = \mathcal{O}(h)$).

One of several effects of the actuation is a distinct periodic tilting of the streaks, as is illustrated in figure 1b. This has been previously observed by means of smoke/laser visualisations by Choi (2002), but the interpretation of the origin of tilting given therein is at variance from the present observations. The orientation approximately follows the phase of the shear angle around $y^+ \sim 10$, as will be shown later in figure 5. The streak angle is also observed to change orientation rapidly, to decay during rapid changes in the strain and to revive when the strain "lingers", the last suggesting the relevance of a streak-amplification time scale. Neither the streaks, nor their re-orientation, appears to be linked to the concept of inclined hair-pin-vortex legs. In particular, there is a remarkable degree of wall-normal uniformity (coherence) in the streak angle across the viscous sublayer, which appears to be disproportionate to the wall-normal variation of the shear induced by the Stokes layer.

Figure 1c illustrates that the streaky structure almost disappears at the close-to-optimum actuation period of $T^+ = 100$, as also found from two-point spanwise correlations, where the first minimum, pertaining to near-wall streaks spacing, has effectively vanished for this period (not shown here). At this state, turbulence levels in the viscous sublayer are significantly weakened, reflecting a decline in wall-normal fluctuations and hence turbulent shear stress. Importantly, the reduction in both turbulence activity and intensity of the streaks is virtually independent of the actuation phase, and this is so at all actuation periods. In other words, the effect of the time-dependent actuation is to progressively and cumulatively weaken the near-wall turbulence activity and the intensity of the streaks, with the wall-averaged streamwise skin-friction being effectively divorced from the temporal variation of the spanwise actuation.

Statistical properties

A global view of the effects of the actuation on the skin friction is conveyed by figure 2. Choi et al. (2002); Quadrio and Ricco (2004) argue that the composite parameter S^+ (defined in Quadrio and Ricco, 2004) can be correlated linearly with the drag-increment level (see figure 2). However, Quadrio and Ricco (2004) have also demonstrated that the correlation does not seem to hold well for actuation periods T^+ greater than 150, as is also illustrated by figure 2. Within the range of conditions examined, the maximum drag decrease is 38.5%, and this is achieved at $T^+ = 100$. At the higher Re_τ value, the maximum suppression is lower, around 32%. Figure 2 shows that the present drag-reduction values are broadly in line with the correlation, as long as T^+ remains near or below the optimal value. The effectiveness of the actuation diminishes rapidly when T^+ rises beyond the optimum value. Indeed, as the actuation approaches a state not dissimilar to a uni-directional wall motion in the spanwise direction, the drag increases slightly.

With attention focusing on the data for $T^+ < 150$, there is a clear indication of a decline in drag-reduction levels with increasing Reynolds number. This lower effectiveness of the actuation at the higher Reynolds number points to a diminishing influence of the processes in the viscous sub-layer on the drag, and (probably) to an increasing impact of larger-scale structures in the outer log-law region, in which the turbulent shear stress rises progressively with Reynolds number towards the wall-shear-stress level, with the high level extending over an increasing range of y^+. A trend thus emerges for a "top-down" influence becoming more important to wall friction with increasing Reynolds number.

Possible reasons for $T^+ = 100$ being close to the most effective value, and for higher values being much less so, will be discussed later. First, the influence of actuation on the statistical fields is considered. To this end, the following triple decomposition for any time-varying quantity a is adopted:

$$a = \bar{a} + \tilde{a} + a'', \; a' = \tilde{a} + a'', \; \langle a \rangle = \bar{a} + \tilde{a} \qquad (1)$$

where $\bar{a}$ is the time-averaged value of a, $\tilde{a}$ is the periodic component, a'' is the stochastic (turbulent) contribution, a' denotes the total fluctuation, and $\langle a \rangle$ is the phase averaged value.

Profiles of stochastic second moments, plotted in terms of inner scaling, are shown in figure 3. Although not obvious, because scaling is based on the actual u_τ value, the general response to the actuation is a substantial decline, especially close to the wall, of all the normal stresses and the shear stress. At the close-to-optimum actuation period, all stresses reduce by at least 30% throughout the entire channel height. Most important is the decrease in the wall-normal stress – up to 80% in the viscous sublayer – as this is primarily responsible for the production of the shear stress (through $-\overline{v''v''}\,\mathrm{d}\bar{u}/\mathrm{d}y$). This reduction in turbulence levels is accompanied by a thickening of the viscous sublayer, indicating that the flow is driven towards a laminar state. One further important response of the flow to the actuation, conveyed by figure 3, is the progressive convergence of u'' and w'' as T^+ is increased.

This is due to two effects. First, as will be shown below, by reference to budgets, the Stokes-layer strain causes an extra production term for $\overline{w''w''}$, which reaches a maximum

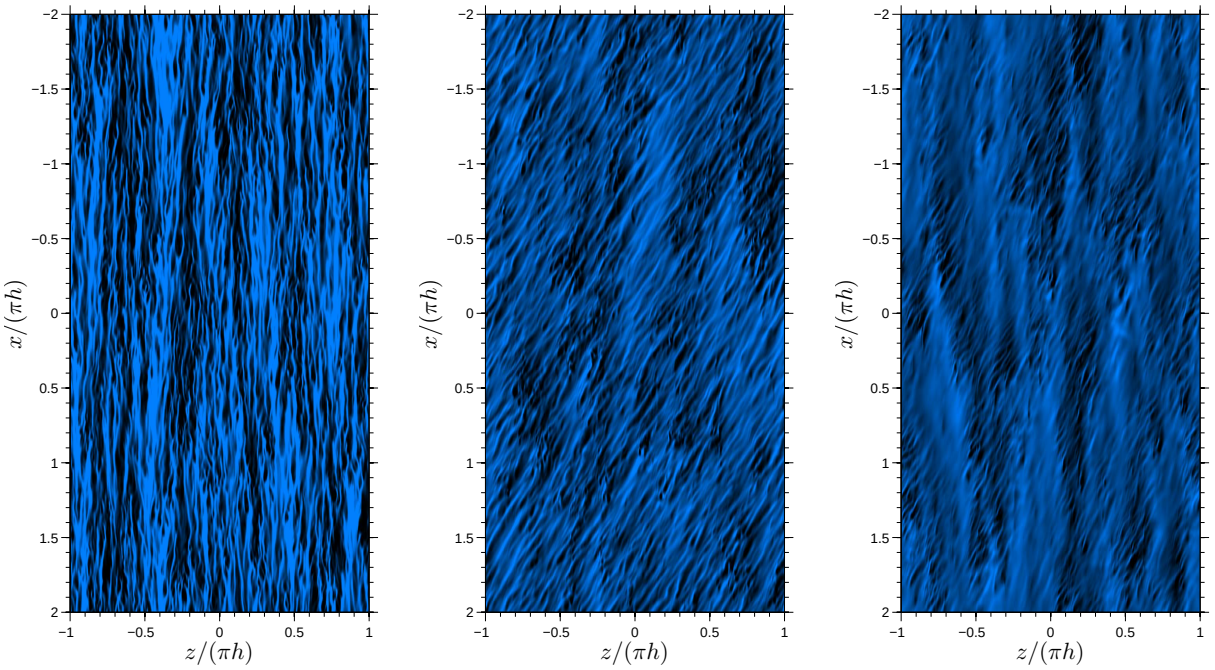

(a) forcing off (b) forcing on, $T^+ = 200$ (c) forcing on, $T^+ = 100$

Figure 1: Instantaneous snapshots of the streamwise velocity fluctuations u' at $y^+ \approx 6$. The same colormap is applied to (a), (b) and (c) after clipping the data to $u'/U_{\text{bulk}} \in [-0.12, 0.45]$. Blue (bright) regions correspond to pronounced velocity deficits relative to the mean value. Note the virtual absence of small-scale streaks in (c), where the skin friction drops by 32% (25% in (b))

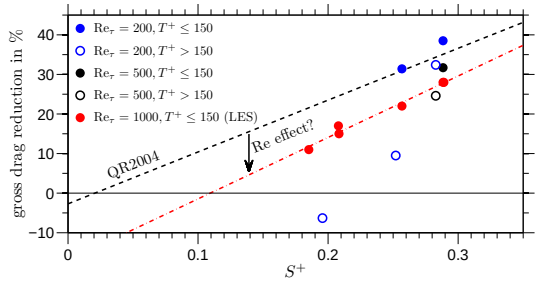

Figure 2: Composite-parameter S^+ correlation with drag-reduction levels. The line labelled "QR2004" corresponds to the best fit line ($\%P_{sav} = 131S^+ - 2.7$) from Quadrio and Ricco (2004). The DNS and LES data at $Re_\tau = 200$ and $Re_\tau = 1000$ are from the present authors

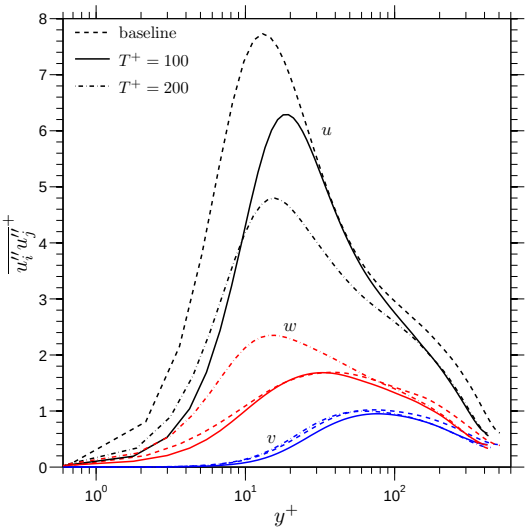

Figure 3: Reynolds-stress tensor normal components based on stochastic velocity fluctuations (in actual wall units)

around $y^+ \sim 10$, and which is a significant (indeed, a major) contributor to the budget of the spanwise stress $\overline{w''w''}$ at $T^+ = 200$. At $T^+ = 100$, this production is much lower, because the wall-normal fluctuations are much weaker. Second, the spanwise forcing introduced a periodic realignment of the streaks (figure 1). This gives rise to a spanwise component of the streak-oriented fluctuations and thus to an enhancement of the spanwise stress as well as to a reduction in the streamwise fluctuations. Again, the effect is weaker at $T^+ = 100$, as the streaks are much weaker.

Of the complete set of budgets available and to be reported in Touber and Leschziner (2011), only two are included and discussed herein, namely for $\overline{v''v''}$ and $\overline{w''w''}$. The corresponding equations are:

sponding equations are:

$$\frac{\partial \overline{v''v''v''}}{\partial y} = -2\overline{v''\frac{\partial p''}{\partial y}} - \frac{2}{Re}\sum_{i=1}^{3}\overline{\left(\frac{\partial v''}{\partial x_i}\right)^2} + \frac{1}{Re}\frac{\partial^2 \overline{v''v''}}{\partial y^2} \quad (2)$$

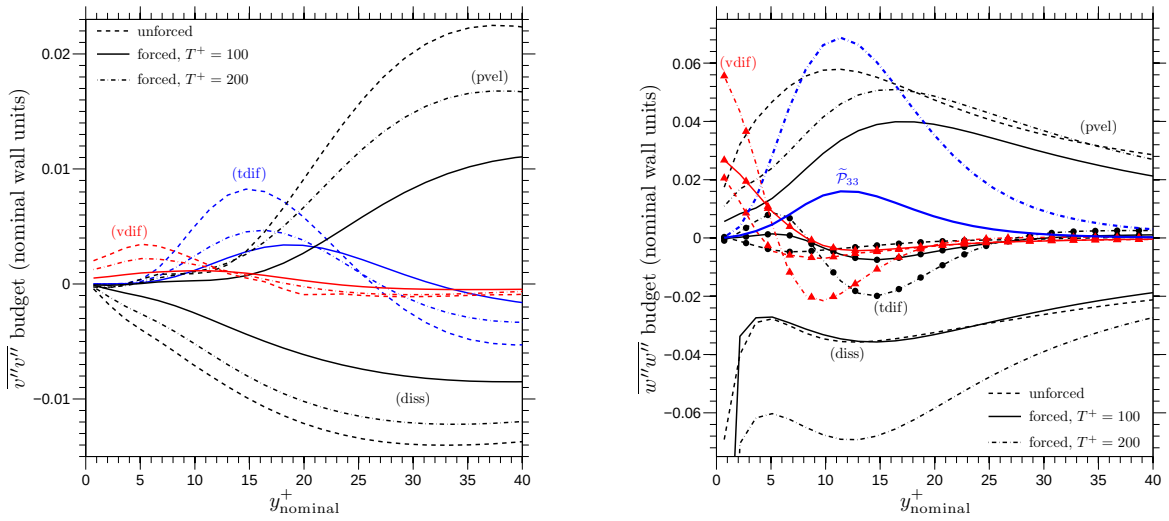

(a) $\overline{v''v''}$ budget

(b) $\overline{w''w''}$ budget

Figure 4: Budgets of $\overline{v''v''}$ and $\overline{w''w''}$ scaled using the baseline friction velocity – (tdif) turbulent diffusion, (pvel) pressure-velocity, (diss) dissipation and (vdif) viscous diffusion

$$\frac{\partial \overline{w''w''v''}}{\partial y} = -2\overline{w''\frac{\partial p''}{\partial z}} \underbrace{-2\overline{\langle w''v''\rangle \frac{\partial \tilde{w}}{\partial y}}}_{\widetilde{\mathcal{P}}_{33}} - \frac{2}{Re}\sum_{i=1}^{3}\overline{\left(\frac{\partial w''}{\partial x_i}\right)^2} + \frac{1}{Re}\frac{\partial^2 \overline{w''w''}}{\partial y^2} \quad (3)$$

A key feature of equation 2 is that its only connection with other equations is via the pressure-velocity interaction term. As is shown in figure 4a, this term feeds energy into $\overline{v''v''}$ *above* the viscous sublayer, with dissipation and turbulent diffusion providing the bulk of the balance. Remarkably, it is diffusion that is responsible for feeding $\overline{v''v''}$ into the viscous sublayer, in response to the pressure-velocity process outside this layer. Very close to the wall, viscous diffusion takes over this role. Forcing is seen to substantially reduce the pressure-velocity term. Dissipation declines to a lesser extent, and thus turbulent diffusion has to reduce materially. Within the viscous sublayer, the pressure-velocity term is a minor contributor, but there is nevertheless a noteworthy decline in this term, especially at $T^+ = 100$ (about 75% relative to the unforced case). In the presence of forcing, the strong decrease in the pressure-velocity interaction also depresses the diffusion process and hence the near-wall level of $\overline{v''v''}$.

The depression in the pressure-velocity term in the $\overline{v''v''}$ budget is, arguably, at the heart of the drag-reduction process. An analysis not reported herein shows that forcing reduces markedly the wall-normal gradient of the stochastic pressure fluctuations. This, as well as studies of structural features reported below, suggest that the strong (unsteady) shearing produced by the Stokes motion *shields* the near-wall region from eddies penetrating from the outer region, thus depressing the pressure-velocity interaction.

The budget for $\overline{w''w''}$ is shown in figure 4b. Its most interesting feature is the large production $\widetilde{\mathcal{P}}_{33}$ due to the Stokes motion. This is especially high at $T^+ = 200$, as a consequence of the combination of higher Stokes straining and $\langle w''v''\rangle$ levels in the upper part of the viscous layer, the latter reflecting the elevation of w'' by the Stokes strain. This production is responsible for the peak in $\overline{w''w''}$ seen in figure 3. It will also be shown later how the periodic actuation generates peaks in $\overline{w''w''}$ when the gradient of the Stokes motion periodically reaches a maximum. Predictably, the response of this production is a substantial elevation in the diffusion process, both transferring $\overline{w''w''}$ from the high-production region towards the wall, and of the dissipation process, followed by a decline in all the above terms as the production diminishes strongly at $T^+ = 100$. Interestingly, the pressure-velocity contribution seems to be essentially decoupled from the production, insofar as the former declines monotonically with forcing, despite the introduction of production.

Insights from near-wall structures

The response of the streaks to forcing is described, in principle, by the equations governing the stochastic fluctuations. These are not given here in detail. In the context of a double-periodic channel flow, two terms that are of particular relevance to the behaviour of the streaks are $v''\mathrm{d}\bar{u}/\mathrm{d}y$ in the u'' equation and $v''\partial\tilde{w}/\partial y$ in the w'' equation. The former is associated with the streak-generation process in an unforced flow. For a low-velocity streak, like in figure 7a, $u'' < 0$, $v'' > 0$, and $v''\mathrm{d}\bar{u}/\mathrm{d}y > 0$, will tend to further reduce u'', thus enhancing the streak strength. This amplification is one important constituent in the paradigm proposed by Chernyshenko and Baig (2005), also involving convection and diffusion and inter-component redistribution, to explain the streak-generation mechanism. Based on this argument, streaks are expected to align with the mean shear $\mathrm{d}\bar{u}/\mathrm{d}y$, as they indeed do in canonical channel flows (see figure 1a), and

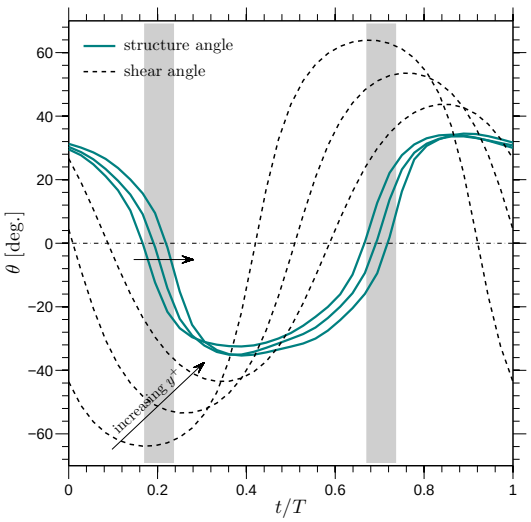

Figure 5: Streak and shear angles as a function of phase for $y^+ \in \{2, 6, 10\}$ and $T^+ = 200$

not necessarily with the flow direction. Of course, in the baseline case, mean-shear and flow directions coincide.

With actuation turned on, term $\tilde{w}$ is seen to take a role similar to $\overline{u}$ and thus to have an analogous impact on the streak-generation process. However, $\tilde{w}$ and $\partial\tilde{w}/\partial y$ are periodic, change sign, and do so at different phase values. Therefore, while the role of $\tilde{w}$ is mathematically similar to the one of $\overline{u}$, its capacity to generate streaks is altered by the temporal dependence and the sign changes. Moreover, the amplitude of $\partial\tilde{w}/\partial y$ at the wall for the actuation values considered here can be up to three times larger than that of $\mathrm{d}\overline{u}/\mathrm{d}y$, so the former will make a significant contribution to the streak-formation process.

If streaks are generated through the combination of a wall-normal disturbance with the "mean" wall-normal shear, forced channel flows should feature streaky patterns aligned with the local phase-averaged shear vector $(\mathrm{d}\overline{u}/\mathrm{d}y, \partial\tilde{w}/\partial y)$ formed on any wall-parallel plane. This is indeed shown in figure 5, where the angle of the most energetic streaks in the DNS were extracted and compared with the phase-averaged shear-vector direction. As already highlighted, streaks align with the shear at $y^+ \approx \mathcal{O}(10)$ and show a high degree of wall-normal coherence. The fact that the alignment deteriorates in the bottom part of the viscous sublayer reflects the weak production very close to the wall, because of the extremely low v''. For both streamwise and Stokes motion, the shear is maximum at the wall and decays rapidly away from the wall (exponentially in the case of $\partial\tilde{w}/\partial y$), while v'' vanishes at the wall. The production maxima are therefore not at the wall but somewhere around $y^+ \sim 10$. Thus, the streak generation process is the strongest around that layer and dominates the streaky pattern across the entire viscous sublayer. This is also why streaks re-orientation is relatively coherent across the viscous sublayer

The periodicity of the spanwise shear means that the streak-amplification process is likely to be sensitive to the ratio of the respective time scales. If the periodic component $\partial\tilde{w}/\partial y$ changes significantly over a shorter period of time than the amplification mechanism, the streaky structures are not given the opportunity to grow and form. In the case of a canonical channel flow, the amplification timescale τ_a^+ is of the order of 50[1]. The periodic transverse component $\partial\tilde{w}/\partial y$ varies in time as shown in figure 5. It is readily recognised that this strain is approximately constant for the longest time about its extrema. If $\tau_s = \{t \in [0,T] : \partial\tilde{w}(y_p)/\partial y > r \cdot \max[\partial\tilde{w}(y_p)/\partial y]\}$, where r is say 0.9 and $y_p^+ = 10$, then the requirement is $\tau_s > \tau_a$ for the streaks to form. Based on figure 5, $\tau_s/T \sim 1/4$ and therefore for $T^+ = 100$ and 200, $\tau_s^+ \sim 25$ and 50, respectively. With $\tau_a^+ \sim 50$, $T^+ = 100$ is not expected to allow enough time for the amplification to occur and the near-wall streaks are not visible, as demonstrated in figure 1c. With $T^+ = 200$, streaks have just enough time to form and grow when $\partial\tilde{w}/\partial y$ is near its extrema and the pattern shown in figure 1b is clearly visible, just before fast-changing $\partial\tilde{w}/\partial y$ disrupt it again.

The choice of actuation period is not only important in allowing the amplification mechanism to occur, but it is also crucial for the requisite variation of $\partial\tilde{w}/\partial y$ in the viscous sublayer. For very small T^+ values, the strain is high at the wall, but the Stokes layer does not penetrate far enough to generate significant cross-flow straining at $y^+ \sim 10$. As T^+ is increased, the Stokes layer thickens and penetrates further out, but the amplitude of the strain rate declines at the wall.

Figure 1 brought to light the presence of two disparate sets of streaks, the more widely spaced residing in the outer turbulent region. The fact that the two sets interact is brought out in figure 6, where large-scale structures and small-scale structures have been separated by filtering, and then brought back into one composite plot where near-wall streaks are lighten up depending on the presence of large-scale structures. Small-scale streaks are mostly inclined following the blue arrow (where "mostly" is based on spectral-energy considerations to be reported in Touber and Leschziner, 2011), but there exist patches where the streaks are more aligned with the orange vector, representing $(\mathrm{d}\overline{u}/\mathrm{d}y, \partial\tilde{w}/\partial y)$. The patches are found to coincide relatively well with the presence of large-scale outer structures, where lighter shades correspond to regions of excess streamwise velocity, therefore indicating events where large-scale regions of flow from above are pushed towards the wall. In such location, the streamwise shear stress is enhanced, effectively reducing the amplification time scale τ_a, thus allowing streaks to form faster and be closely related to the direction of greatest straining. This may be referred to as a *modulation* by the outer structure of the near-wall streak formation, an interaction that is likely to become increasingly important at rising Reynolds number and being responsible for the reduced effectiveness of the control, as indicated in figure 2.

The response of the streaks, in cross-section, may be clarified by performing streak-specific conditional sampling and phase-averaging. A variety of interactions between correlations of stochastic fluctuations and the streak distortions may thus be studied. An example is given in figure 7 in which the deformation of the low-speed streak contours is shown alongside colour contours of the production $v''\partial\tilde{w}/\partial y$ and the Stokes-strain generated spanwise fluctuations. As v'' is pos-

[1] Private communication with Prof. S.I. Chernyshenko and Mr. O. Blesbois (Imperial College London)

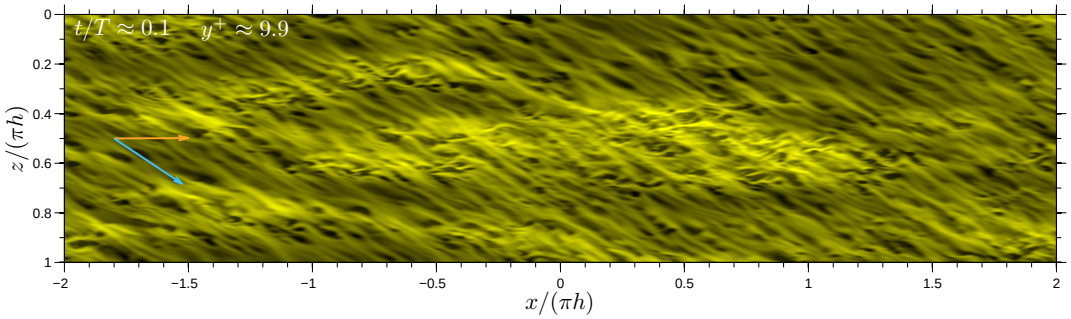

Figure 6: Outer-layer-structure speeding/delaying effects on near-wall streak re-orientation

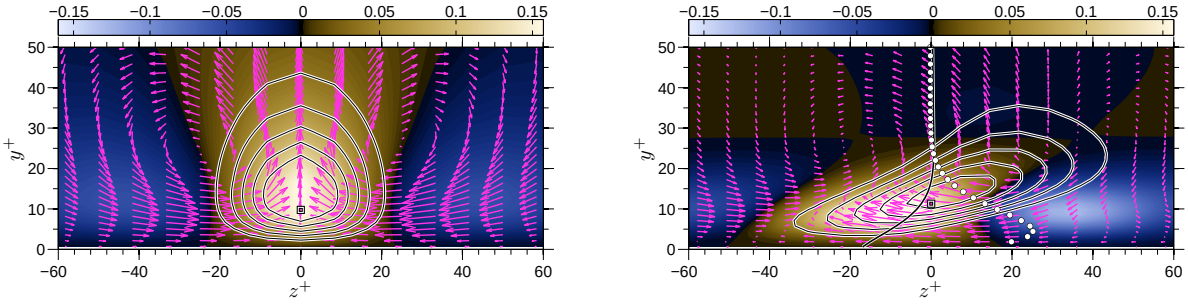

(a) forcing off

(b) forcing on, $T^+ = 200$, $t/T \approx 0.83$

Figure 7: Conditionally-averaged streaks obtained by sampling the flow, after application of a high-pass filter to remove super-streak modulations, such that $u'' < b$ at $y^+ \approx 10$ (black and white square), with $b = -0.20U_{\text{bulk}}$ in (a) and $b = -0.10U_{\text{bulk}}$ in (b). Contour lines give the streamwise velocity contours $u''/u_\tau \in \{-2.4, -2.0, -1.6, -1.2, -0.8\}$. The filled contours in the background give the conditionally-averaged fields of $v''\mathrm{d}\overline{u}/\mathrm{d}y$ in (a) and $v''\partial\tilde{w}/\partial y$ in (b) (in U_{bulk}^2/h units). Vectors give the transverse velocity fields. The phase-averaged spanwise velocity $\tilde{w}$ is indicated by the thick black line and the white dots indicate $\partial\tilde{w}/\partial y$

itive, the spanwise fluctuations oppose the Stokes strain and are broadly aligned with the Stokes motion itself, enhancing the convective distortion of the streaks. The figure shows that the maximum fluctuations occur at $y^+ \sim 10$, at which height the related production also peaks. Analogous plots that include fields of the wall-normal and the shear stress suggest strongly that the large lateral displacement of the low-speed streaks by the combined Stokes and lateral fluctuations, in particular, cause a disruption of wall-normal motion, reduce the shear stress, shield the wall from outer sweeping events and transport low-streamwise-momentum towards the wall, all contributing to the reduction of the turbulent wall-shear stress.

Acknowledgement The authors would like to acknowledge the financial support from EPSRC through grant EP/G061556/1, together with Airbus Operations Ltd and EADS UK Ltd. We are also grateful to Imperial College HPC Service facilities for the access to its high-performance computer cx2.

REFERENCES

S. I. Chernyshenko and M. F. Baig. The mechanism of streak formation in near-wall turbulence. *J. Fluid Mech.*, 544:99–131, 2005.

J.-I. Choi, C.-X. Xu, and H.-J. Sung. Drag reduction by spanwise wall oscillation in wall-bounded turbulent flows. *AIAA Journal*, 40(5), 2002.

K.-S. Choi. Near-wall structure of turbulent boundary layer with spanwise-wall oscillation. *Phys. Fluids*, 14(7), 2002.

G. M. Fishpool and M. A. Leschziner. Stability bounds for explicit fractional-step schemes for the navier–stokes equations at high reynolds number. *Computers & Fluids*, 38: 1289–1298, 2009.

W. J. Jung, N. Mangiavacchi, and R. Akhavan. Suppression of turbulence in wall-bounded flows by high-frequency spanwise oscillations. *Phys. Fluids A*, 4(8):1605–1607, 1992.

M. Quadrio and P. Ricco. Critical assessment of turbulent drag reduction through spanwise wall oscillations. *J. Fluid Mech.*, 521:251–271, 2004.

M. Quadrio, P. Ricco, and C. Viotti. Streamwise-travelling waves of spanwise wall velocity for turbulent drag reduction. *J. Fluid Mech.*, 627:161–178, 2009.

L. Temmerman, M. A. Leschziner, C. P. Mellen, and J. Fröhlich. Investigation of wall-function approximations and subgrid-scale models in large eddy simulation of separated flow in a channel with streamwise periodic constrictions. *International Journal of Heat and Fluid Flow*, 24(2): 157–180, 2003.

E. Touber and M. A. Leschziner. Near-wall streak modifications by spanwise oscillatory wall motions and relationship to friction-drag reduction. To be submitted to J. Fluid Mech., 2011.